Supplementary Information

Real-time correlation of crystallization and segmental order in conjugated polymers

Shaochuan Luo,[abc] Yukun Li,[b] Nan Li,[c] Zhiqiang Cao,[d] Song Zhang,[d] Michael U. Ocheje,[e] Xiaodan Gu,[d] Simon Rondeau-Gagné,[e] Gi Xue,[b] Sihong Wang,[cf] Dongshan Zhou,[b] and Jie Xu,*[cf]*

[a] School of Chemistry and Chemical Engineering, Nanjing University of Science and Technology, Nanjing, 210094 P. R. China.

[b] Department of Polymer Science and Engineering, State Key Laboratory of Coordination Chemistry, Key Laboratory of High Performance Polymer Material and Technology, MOE, School of Chemistry and Chemical Engineering, Nanjing University, Nanjing, Jiangsu 210023, China.

[c] Pritzker School of Molecular Engineering, University of Chicago, Chicago, Illinois 60637, United States.

[d] School of Polymer Science and Engineering, Center for Optoelectronic Materials and Devices, University of Southern Mississippi, Hattiesburg, Mississippi 39406, United States.

[e] Department of Chemistry and Biochemistry, University of Windsor, Windsor, Ontario N9B3P4, Canada.

[f] Nanoscience and Technology Division, Argonne National Laboratory, Lemont, Illinois 60439, United States

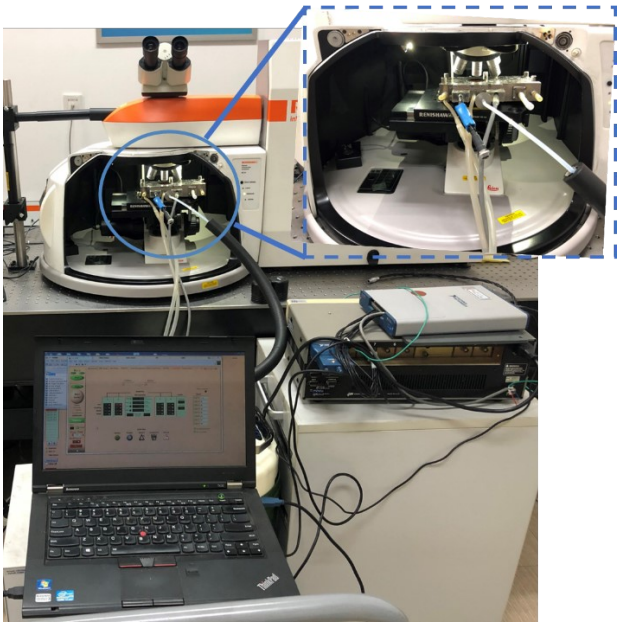

Figure S1. The integration of stage-type FSC with Micro-Raman spectroscopy.

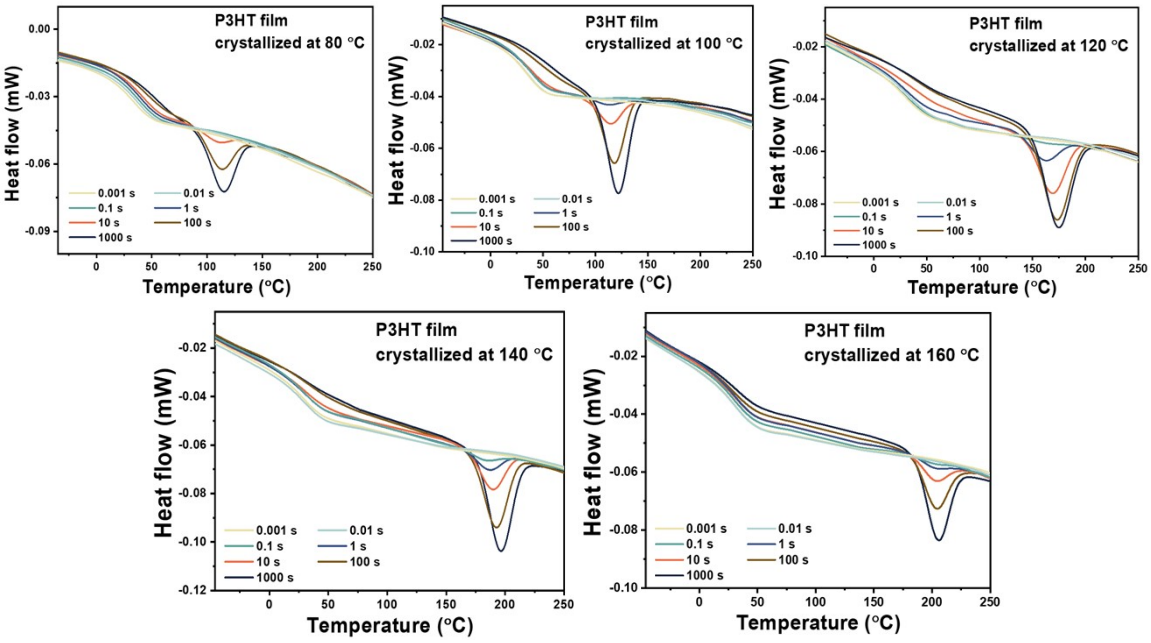

Figure S2. Reheating of P3HT film after crystallized at different temperatures for different time.

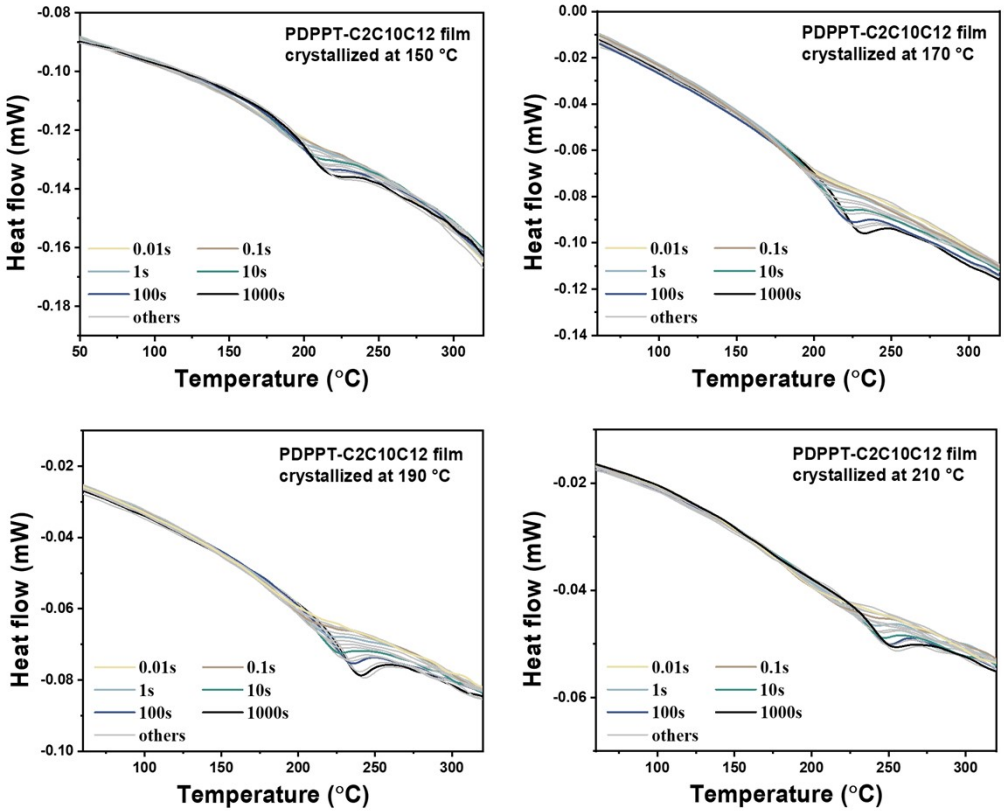

Figure S3. Reheating of PDPPTC2C10C12 film after crystallized at different temperatures for different time.

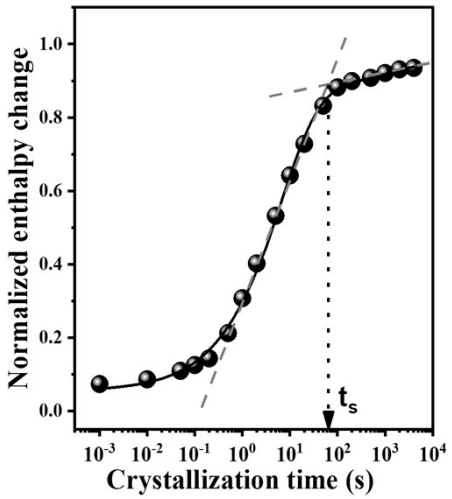

Figure S4. The definition of the ts.

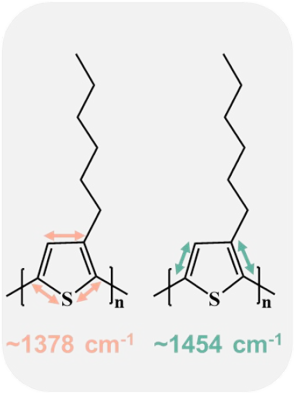

Figure S5. Diagram illustrating the dominant bond stretches associated with the main Raman-active vibrational modes of the P3HT film.

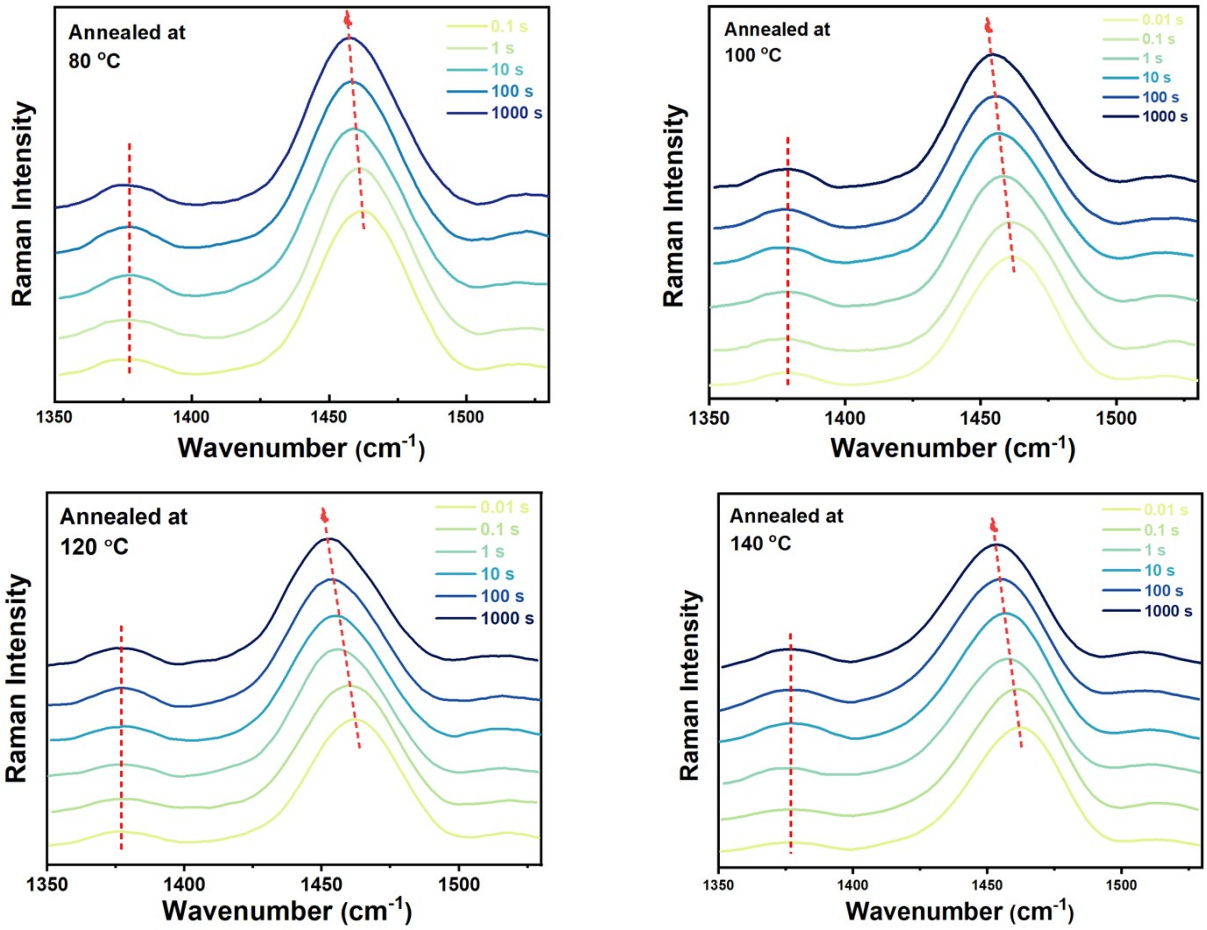

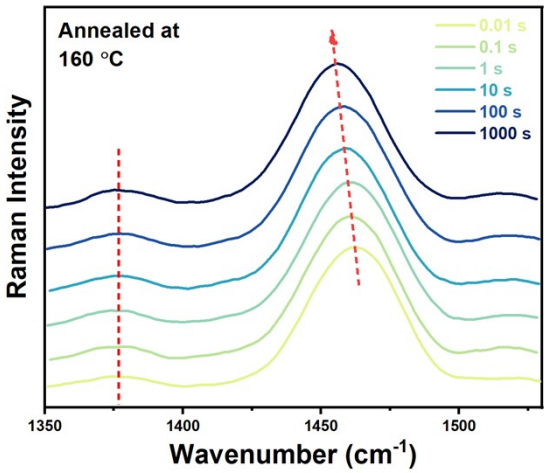

Figure S6. Resonance Raman spectra of P3HT film crystallized at different temperatures for different time.

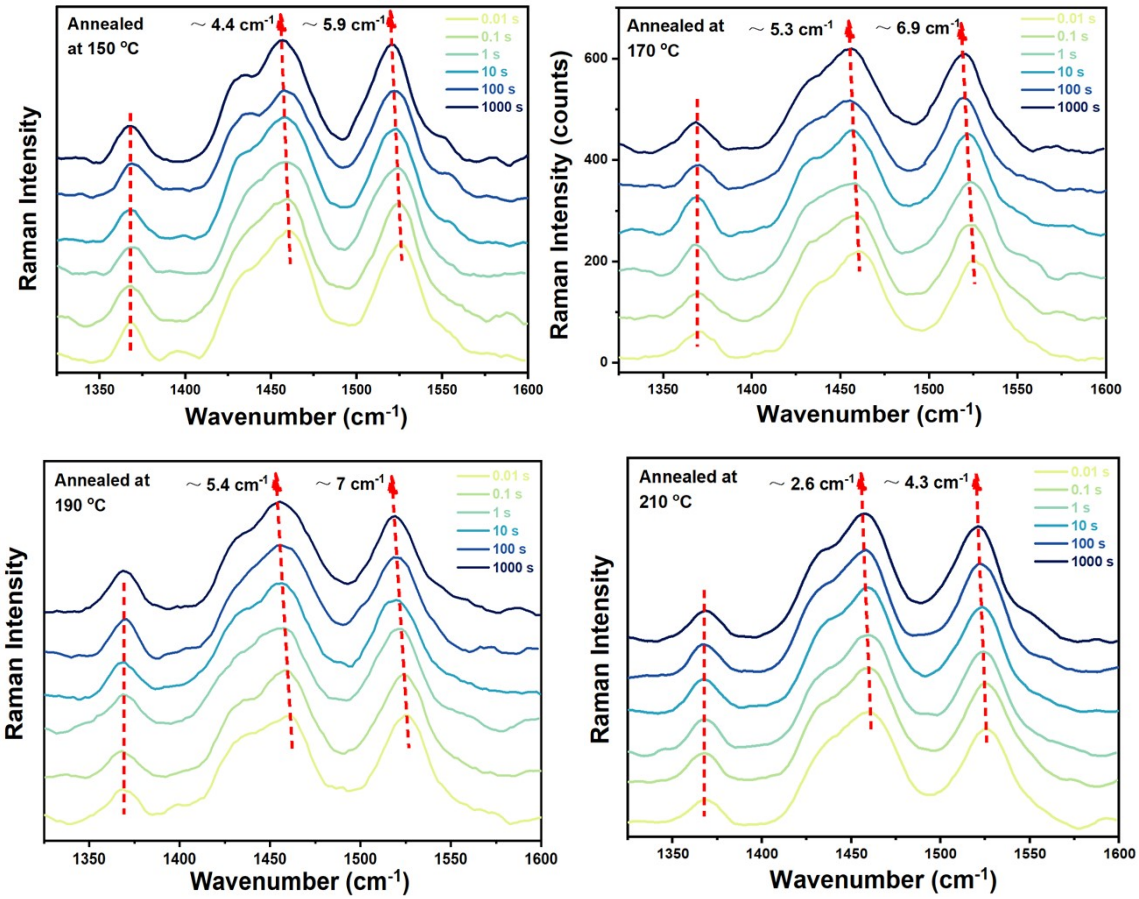

Figure S7. Resonance Raman spectra of PDPPTC2C10C12 film crystallized at different temperatures for different time.

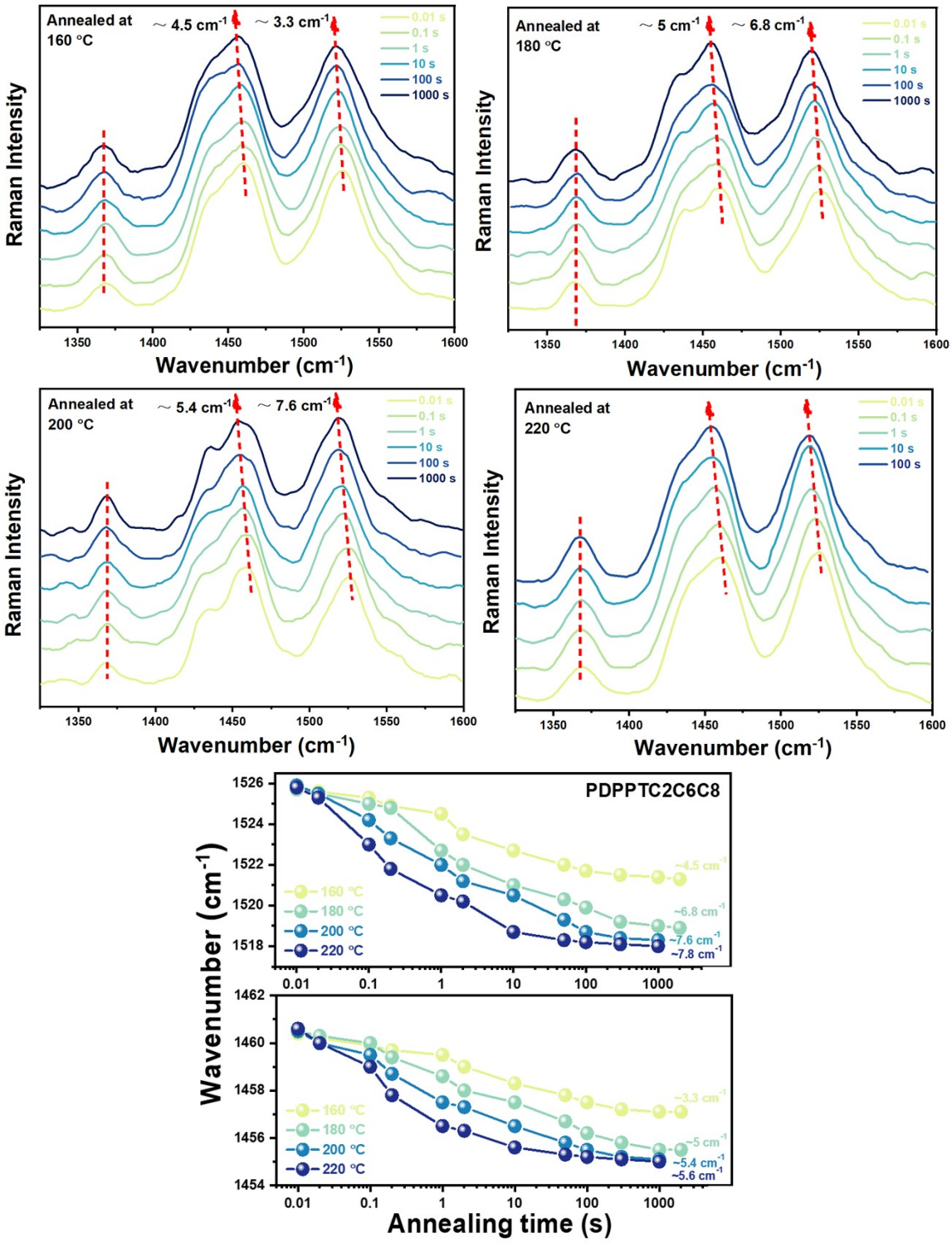

Figure S8. Raman spectra of PDPPT-C2C6C8 film crystallized at different temperatures for different time.

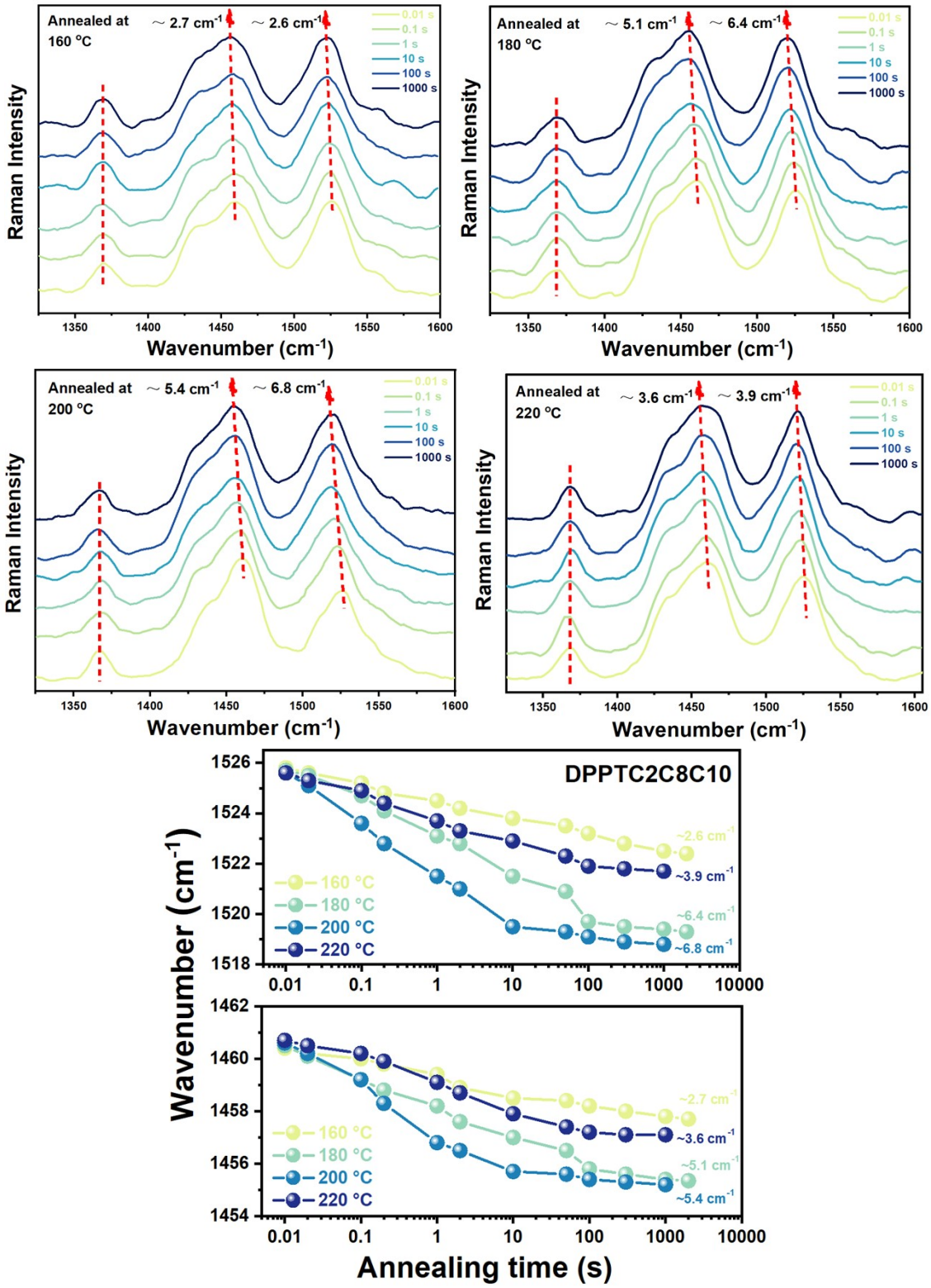

Figure S9. Raman spectra of PDPPT-C2C8C10 film crystallized at different temperatures for different time.

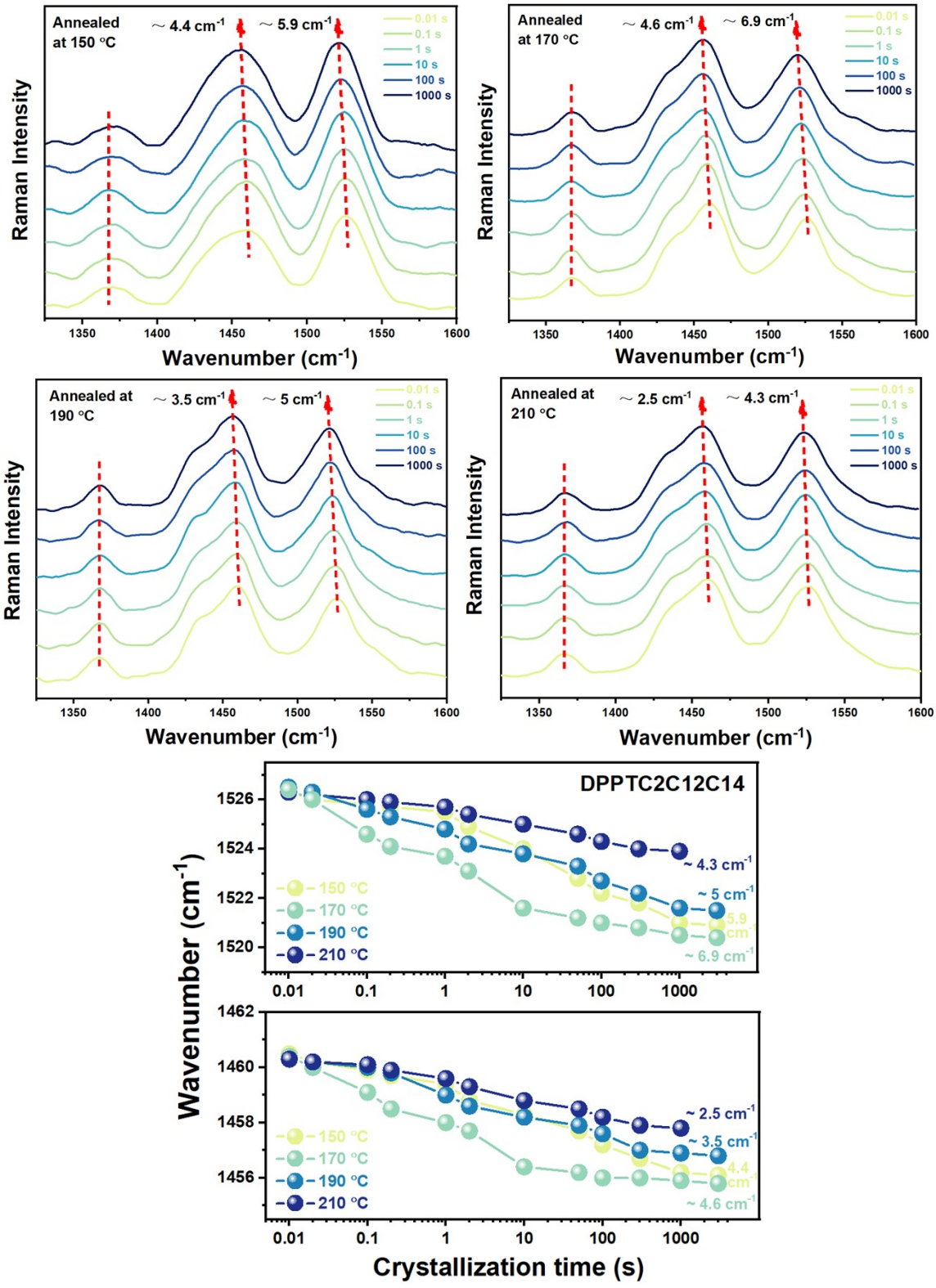

Figure S10. Raman specta of PDPPT-C2C12C14 film crystallized at different temperatures for different time.

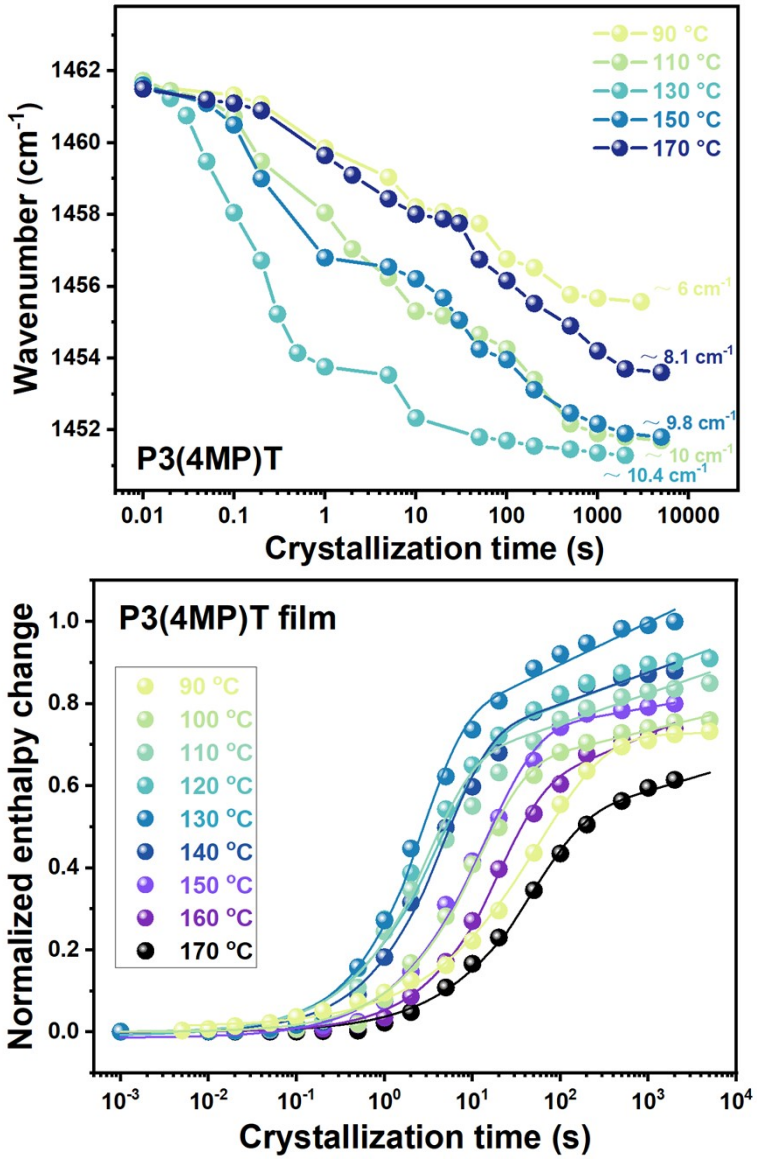

Figure S11. The normalized melting enthalpy change and the wavenumber of C=C mode of P3(4MP)T film crystallized at different temperatures for different time.

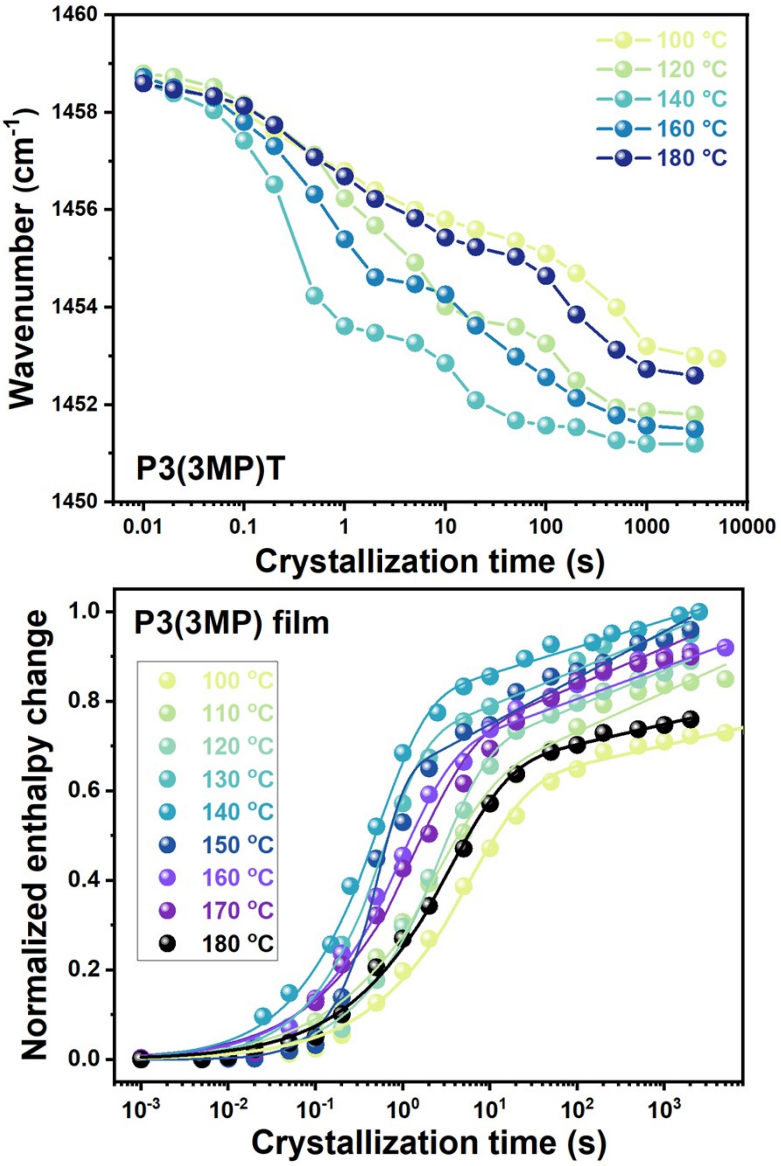

Figure S12. The normalized melting enthalpy change and the wavenumber of C=C mode of P3(3MP)T film crystallized at different temperatures for different time.

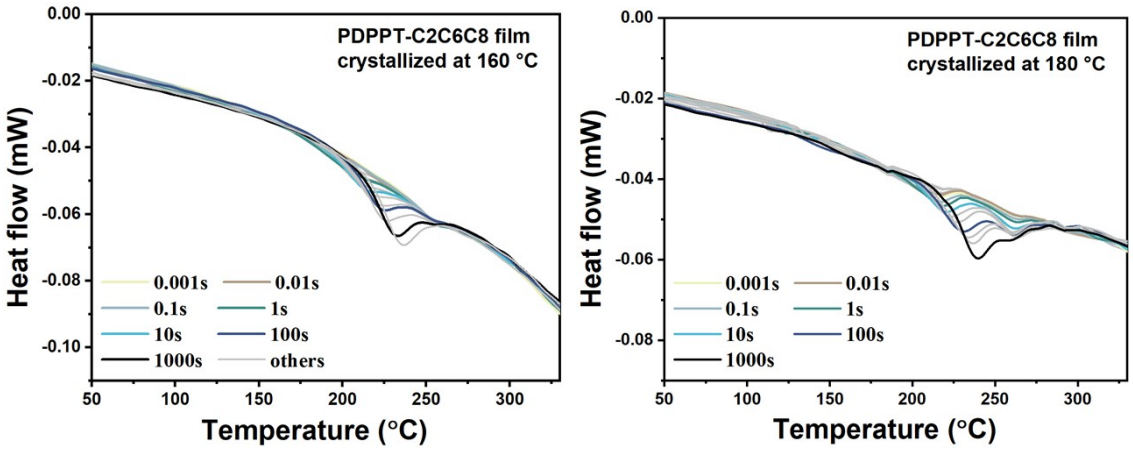

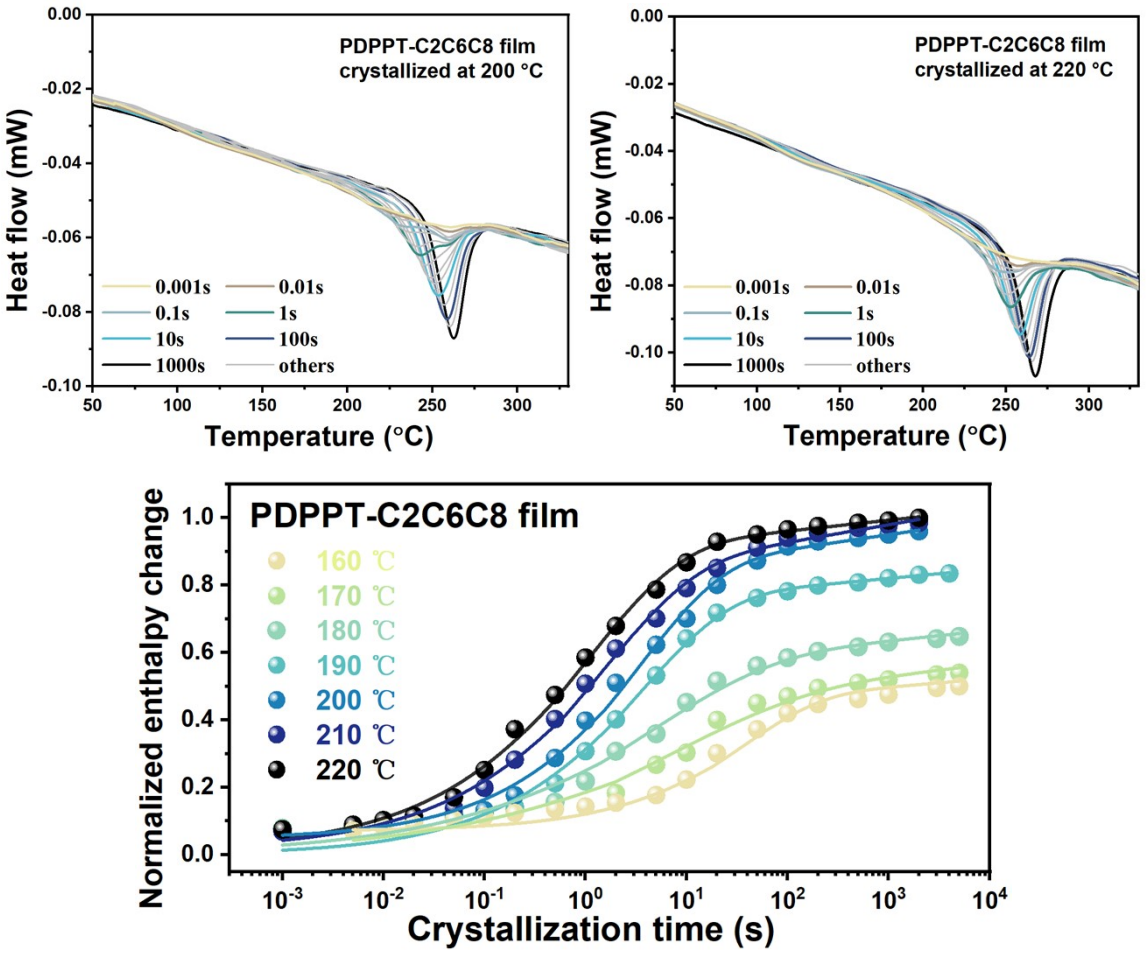

Figure S13. Reheating of PDPPTC2C6C8 film after crystallized at different temperatures for different time. Normalized melting enthalpy change of PDPPT-C2C6C8 film on heating after isothermal crystallization at different temperatures.

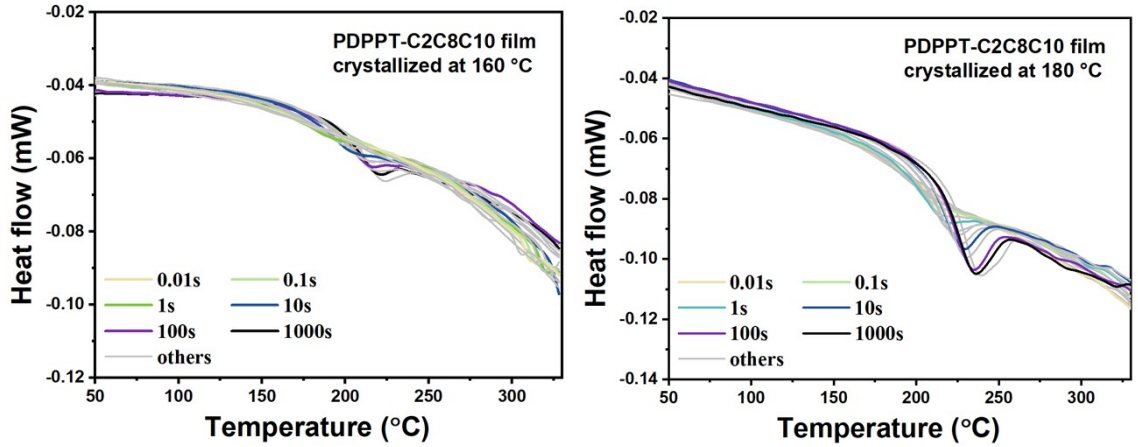

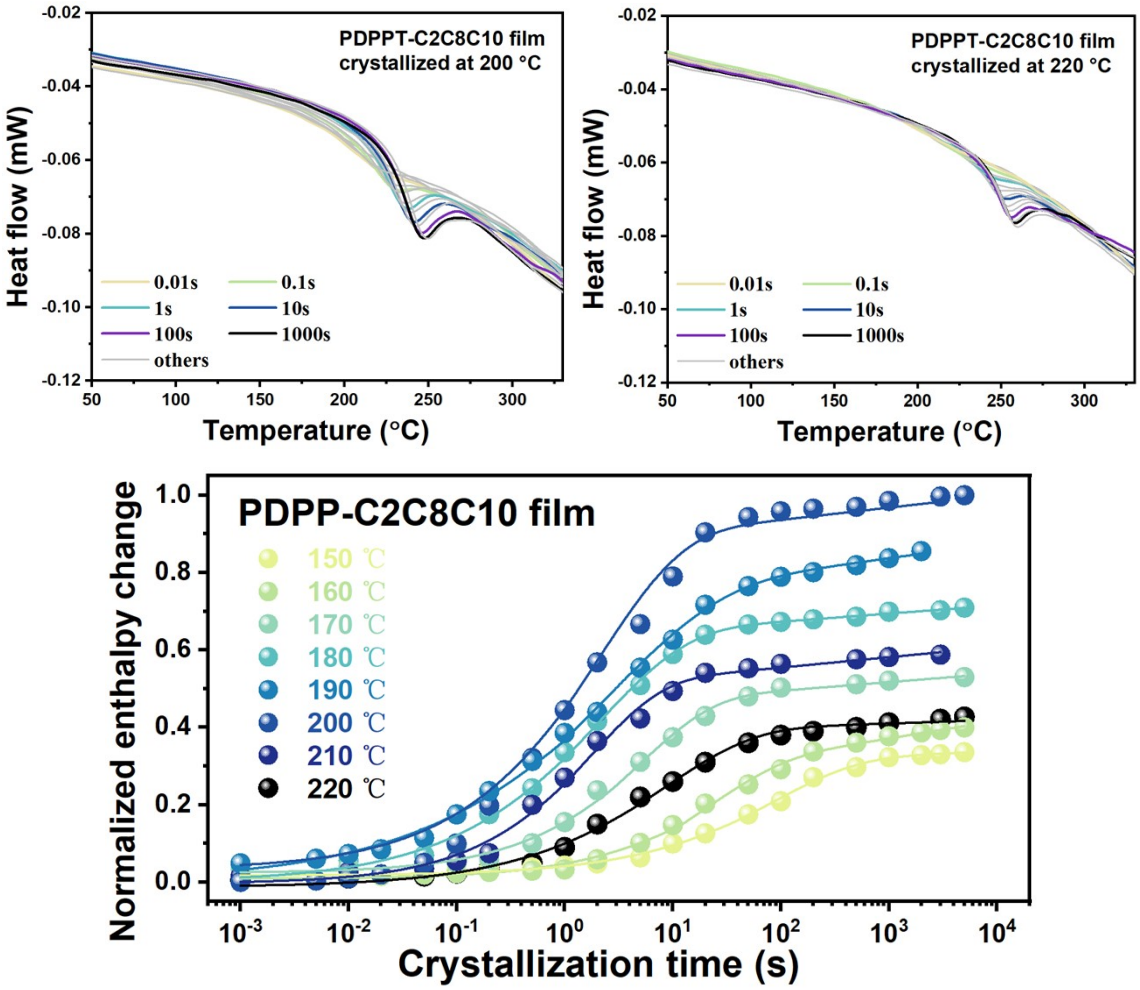

Figure S14. Reheating of PDPPTC2C8C10 film after crystallized at different temperatures for different time. Normalized melting enthalpy change of PDPPT-C2C8C10 film on heating after isothermal crystallization at different temperatures.

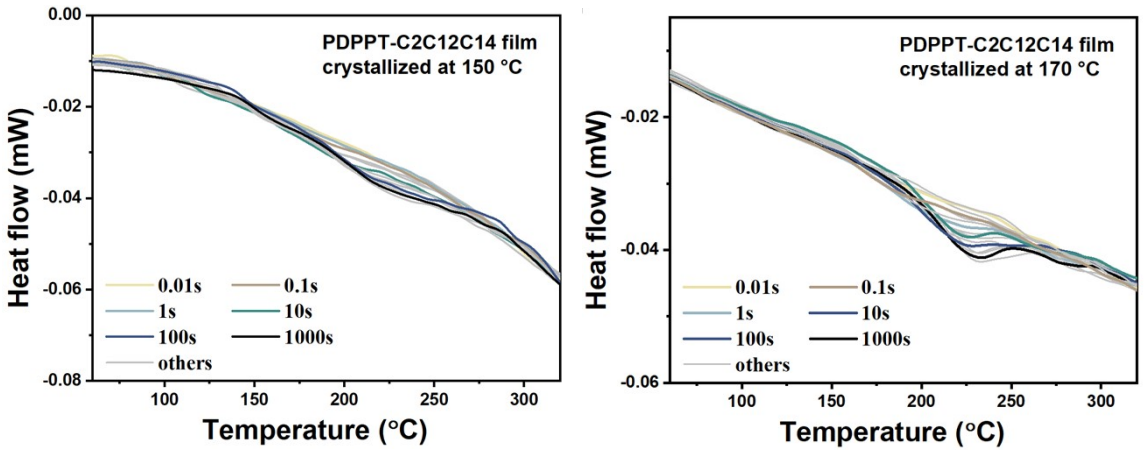

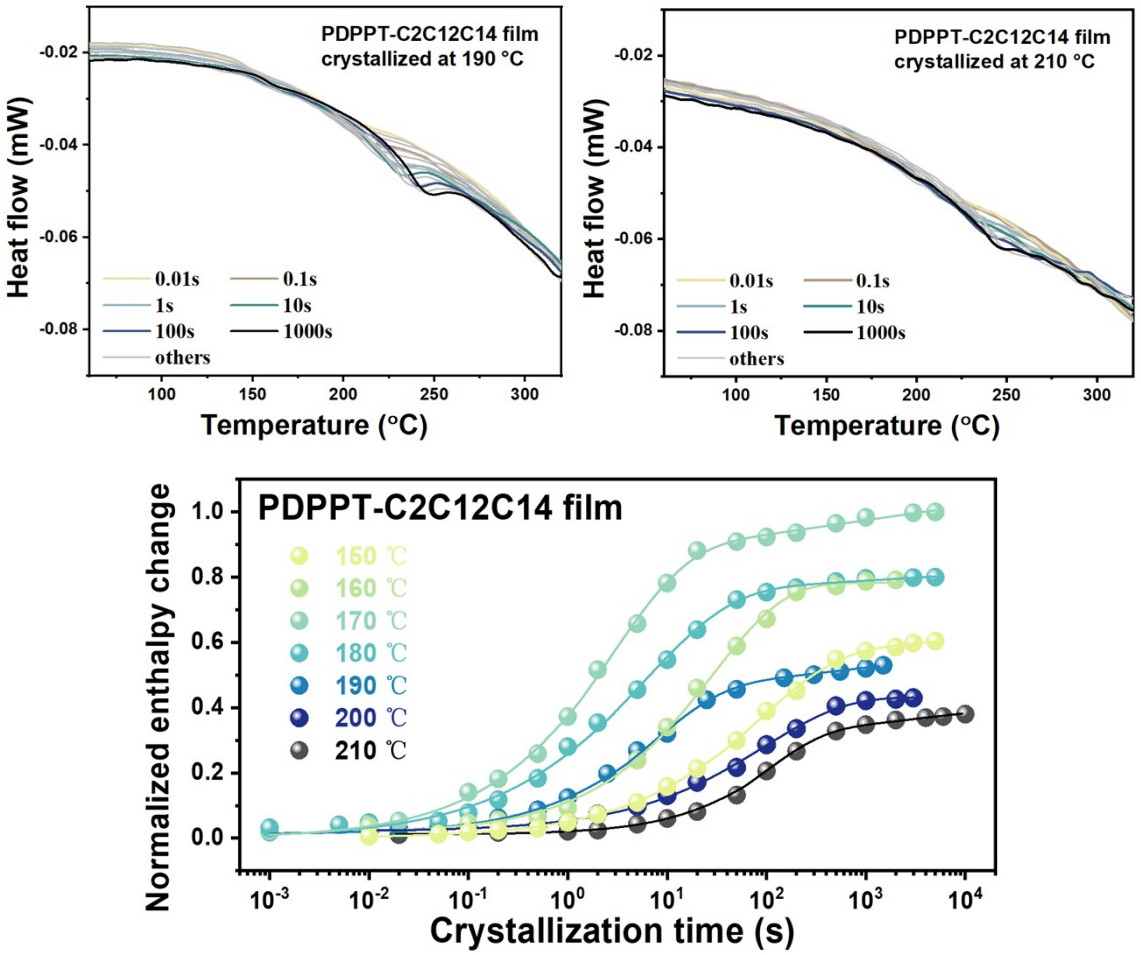

Figure S15. Reheating of PDPPTC2C12C14 film after crystallized at different temperatures for different time. Normalized melting enthalpy change of PDPPT-C2C12C14 film on heating after isothermal crystallization at different temperatures.

Table S1. The saturated wavenumbers of C=C modes and normalized maximum attainable crystallinities of P3ATs and PDPPT-based conjugated polymers crystallized at different temperatures.

Sample	TR I	The saturated wavenumbers of C=C modes	Normalized maximum attainable crystallinities
PDPPT-C2C6C8	T^*-40 °C to T^* (180 °C to 220 °C)	1455.2 ± 0.3 cm^{-1} 1518.3 ± 0.3 cm^{-1}	0.64 to 1
PDPPT-C2C8C10	T^*-20 °C to T^* (180 °C to 200 °C)	1455.3 ± 0.3 cm^{-1} 1519 ± 0.3 cm^{-1}	0.70 to 1
PDPPT-C2C10C12	T^*-30 °C to T^*+10 °C (160 °C to 200 °C)	1455.3 ± 0.3 cm^{-1} 1519.1 ± 0.2 cm^{-1}	0.61 to 1
PDPPT-C2C12C14	T^*-20 °C to T^*+10 °C (150 °C to 180 °C)	1456 ± 0.2 cm^{-1} 1520.6 ± 0.3 cm^{-1}	0.59 to 1
P3HT	T^*-20 °C to T^*+20 °C	1453 ± 0.3 cm^{-1}	0.8 to 1

	(100 °C to 140 °C)		
P3(4MP)T	T*-20 °C to T*+20 °C (110 °C to 150 °C)	1451.5 ± 0.2 cm^{-1}	0.79 to 1
P3(3MP)T	T*-30 °C to T*+30 °C (110 °C to 170 °C)	1451.5± 0.3 cm^{-1}	0.81 to 1

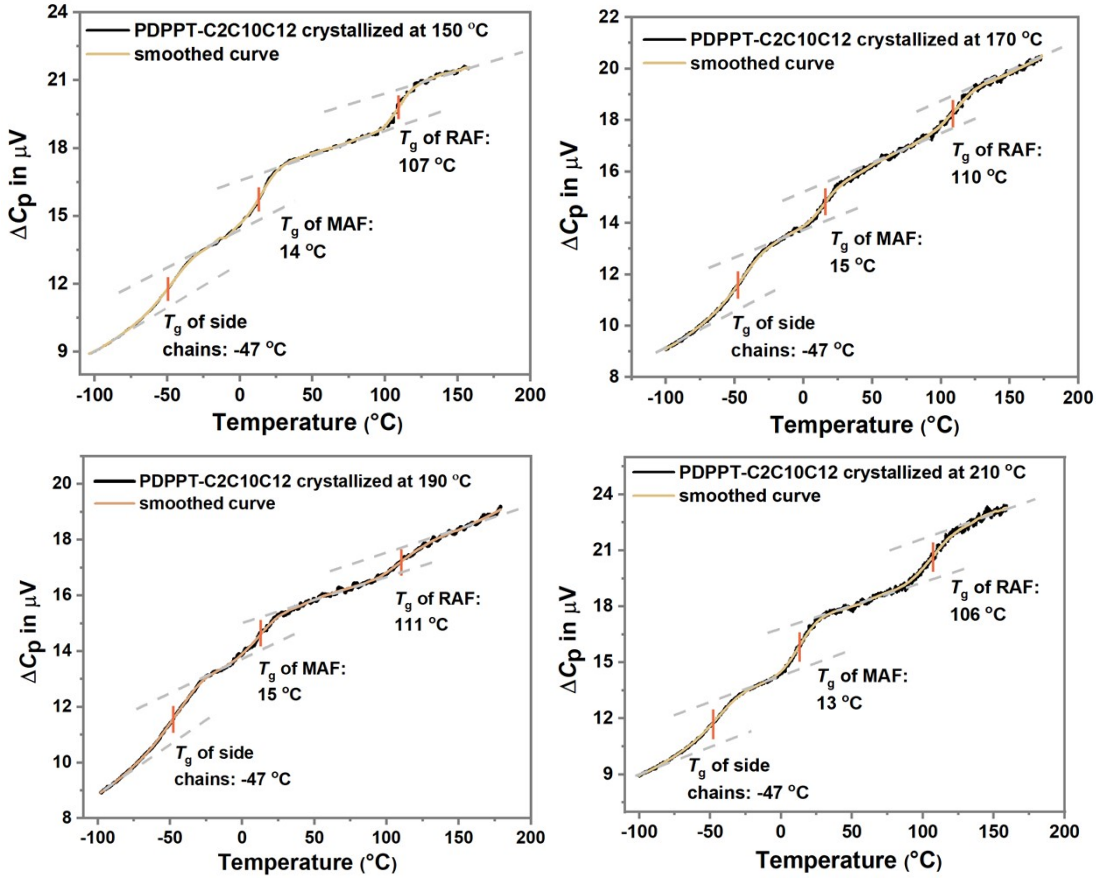

Figure S16. Glass transition behavior of the PDPPT-C2C10C12 film after crystallized at 150 °C, 170 °C, 190 °C and 210 °C.

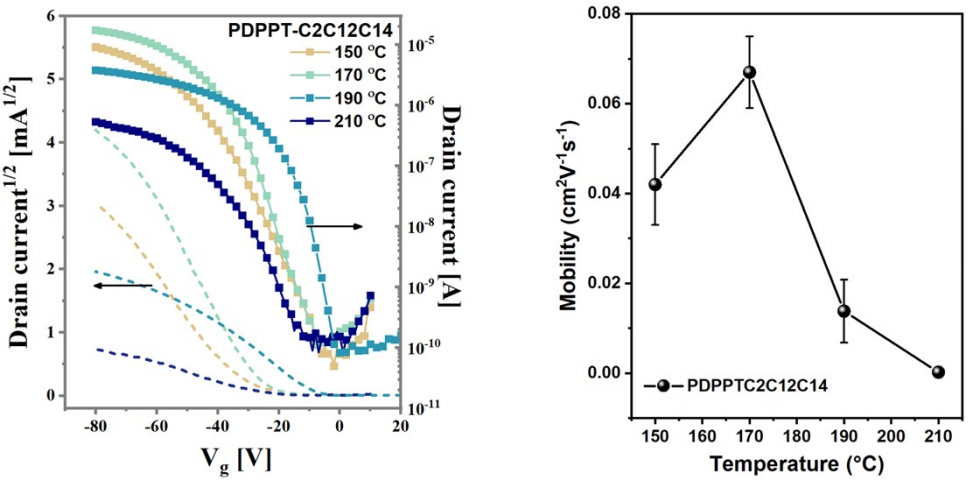

Figure S17. Transfer characteristics and average charge-carrier mobilities for OFET devices of PDPPT-C2C12C14 annealed at different temperatures from amorphous state. After spin coating, films were melted at 300 °C for 1 min and transferred to another hot plate immediately to anneal at different temperatures for 15 min in a N2 filed glove box.

Table S2. Backbone T_g and T_m of P3ATs and PDPPT-based conjugated polymers.

Polymers	Backbone T_g (°C)	T_m (°C)
P3HT	20	204
P3(4MP)T	43	218
P3(3MP)T	49	230

Polymers	Backbone $T_{g,m}$ (°C)	Backbone $T_{g,r}$ (°C)	T_m (°C)
PDPPT-C2C6C8	26	118	255
PDPPT-C2C8C10	22	114	245
PDPPT-C2C10C12	15	110	240
PDPPT-C2C12C14	12	105	232